

Modeling Torso Kinematics in Collegiate Baseball Pitchers Using a Damped Torsion Spring Oscillator and its Relationship to Competitive Performance

Charles Arnold

*This work was submitted as part of a course requirement for completion of the BS degree in the Physics Program at RIT and, in its current form, does not appear in any publication external to RIT.**

(Dated: September 1, 2023)

In baseball, the kinetic chain is described as the complex interaction of the lower extremities, core musculature^{1,6}, and upper extremities. In pitching the Kinetic Chain starts with the Ground Reaction Force (GRF) travels up the body in order of lead knee extension, pelvis rotation, thorax rotation, elbow extension, shoulder internal rotation (IR), and finally the hand. The torso acts as an transmitter that transfers the GRF from the lower extremities to the upper extremities. To model torso kinematics of the pitching delivery, a torsion spring will be used from front foot contact FFC to maximum external rotation MER. The model will consist of 2 analysis of a separation angle using the critically damped solution, and the phase portraits of the decoupled differential equation of the torsion spring. The relationship amongst pitch type and the damping constant showed statistical significance with a p-value of 0.02. There are no statistical correlations amongst the damping constant and key performance indicators (KPI).

Introduction

In Baseball pitching, the kinetic chain starts from the ground reaction force (GRF) created from the front foot contact (FFC) of the lead leg⁸. The GRF travels up through lead leg (by knee extension) into pelvis rotation, following thoracic rotation. When the pelvis rotates independently of the thorax, the athlete creates an elastic force, caused by the external obliques and rectus abdominus muscles, that accelerates their body and arm faster through the motion. This reaction is most commonly called separation. When separation is achieved between the pelvis and thorax, the energy within in the system is maximized by converting the linear GRF into a rotational force between the pelvis and the thorax. In this study, the torso is defined by the pelvis and thorax as independent bodies that make one system. Through separation, the torso acts as a transmitter in order to move the energy from the lower extremities to the upper extremities⁴. By utilizing separation of the torso, the arm can utilize the stretch-shortening-cycle to further accelerate through the following movements: maximum external rotation (MER), internal rotation (IR), and elbow extension. Finally the hand accelerates the ball during ball release (BR).

In baseball, optimal energy transfer is not well understood as it relates to the kinetic chain of the pitching delivery. This is partially due to lack of technology evaluating competitive biomechanics versus controlled laboratory studies which lack representative conditions to games. Many players struggle to sequence the kinetic chain correctly, as somewhere along the chain there is a leak of energy. Inefficient rotational timing, as well as altered acceleration and deceleration of the torso, would represent the largest segment impacting energy flow from the ground to throwing arm. A detailed understanding of torso kinematics that can be captured without laboratory constraints can determine biomechanical consequences that lead to poor performance and injury risk in



FIG. 1: Visualization of the kinetic chain for the pitching delivery. energy starts at there ground and travels up the chain into ball release

the sport. Effects of poor performance can vary from a decrease in ball kinematics to more stress and torques on joint segments of the body. Recent studies have shown an increase of more than 50% in the number of ulnar collateral ligament (UCL) reconstructions performed on high school-aged and younger athletes^{5,8}.

To simplify the kinematics of the torso during the pitching delivery, a torsion spring will model the rotation of the pitching delivery between front foot contact (FFC) and maximum external rotation (MER). During FFC, the pelvis will have reached maximum angular velocity and the thorax will be static, thus creating a separation angle of the torso. During MER, the thorax will have reached maximum angular velocity, and separation angle will approach 0° using the critically damped solution for our model. The torsion force exerted onto the pelvis is caused by the extension of the lead knee. This impulse from the lead knee initiates the pelvis into peak rotation, while the upper extremities separates from the pelvis and does not rotate with the pelvis. This allows us to model the energy flow between time of max pelvis velocity, and max thorax velocity. By increasing efficiency of the trunk, the amount of stress and torque exerted on

the shoulder and elbow will decrease while maintaining higher ball velocities.

In this experiment we are looking to analyse the torso mechanics of the pitching motion using energetics with our 2-part model of the torso. This study has 3 aims:

1. Develop a mathematical model that describe the kinematic rotation of a Pitcher's torso
2. Compare critically damping effects to key performance indicators (KPI's)
3. Compare phase portraits to the separation angle as a function of time

Theory

In this study, the body will be comprised of only the torso as a critically damped torsion spring. For this model, the energy of the torsion spring is conserved. Internal factors such as heat dissipation and absorption by the muscles will not be considered for the model. Movements that are not in the transverse plane such as lateral trunk flexion, which would cause our spring to bend during the throwing motion, will also not be included in the model. By not including these internal and external factors experienced by the torso; therefore only the homogeneous solution is considered. To begin, the model is derived by the standard equation for a damped torsion oscillator

$$I\ddot{\theta} + C\dot{\theta} + K_T\theta = 0 \quad (1)$$

where I is the moment of inertia of the torso, C is the damping coefficient, and K_T is the torsion constant. To solve for the damping constant from FFC to MER, a quadratic expression is used to find the eigenvalues for our system α .

$$\alpha = \frac{-C \pm \sqrt{C^2 - 4K_T I}}{2I} \quad (2)$$

When solving for the critically damped case, the inside of the radical is set to 0. This is because at the $t = MER$, the separation angle is closed to 0° , thus reaching an equilibrium after giving all of its energy to the arm. Solving for the damping constant C gives the following expression in terms of K_T and I .

$$C = \pm\sqrt{4K_T I} \quad (3)$$

When substituting back in for C the new α expression becomes

$$\begin{aligned} \alpha &= \frac{2\sqrt{K_T I}}{2I} \\ &= \sqrt{\frac{K_T}{I}} \end{aligned} \quad (4)$$

After cleaning up the algebra, the eigenvalue for our system is equal to the negative square root of the torsion constant K_T divided by the moment of inertia I .

A dimensionless form of the torsion oscillator will also be used to create a phase portrait of the torsion oscillator. This will demonstrate how each participant, in this study, rotates by comparing individualized phase portrait to corresponding critically damped time series. The dimensionless equation

$$\begin{aligned} \ddot{\theta} + \gamma\dot{\theta} + \theta &= 0 \\ \gamma &= \frac{C}{\sqrt{K_T I}} \end{aligned} \quad (5)$$

is derived when the dimensionless time $\tilde{t} = \sqrt{\frac{K_T}{I}} t$ is substituted into the differential equation. When solving for the critically damped value of γ , a quadratic equation is formed to solve for the inside component of the radical. For the critically damped case, $\gamma = 2$ and when substituted back in, $\alpha = -1$

$$\begin{aligned} \alpha &= \frac{-\gamma \pm \sqrt{\gamma^2 - 4}}{2} \\ \gamma^2 - 4 &= 0 \end{aligned} \quad (6)$$

After theoretically solving for the value of γ , a phase portrait will be constructed by decoupling the second order differential equation into 2 first order differential equations, where μ is the variable that decouples the first derivative from the second derivative.

$$\begin{aligned} \dot{\theta} &= \mu \\ \dot{\mu} &= -\gamma\mu - \theta \end{aligned} \quad (7)$$

For a human pitcher, K_T and I are completely unknown. Without technology to define the torso's elasticity in the transverse planes and mass distribution, K_T and I cannot be computed on their own, thus a new derivation is needed. In order to derive torso separation, a separation angle θ_{sep} and a separation angular velocity ω_{sep} are defined using the law of superposition of the pelvis and thorax as independent bodies.

$$\begin{aligned} \theta_{sep} &= \theta_p - \theta_T \\ \omega_{sep} &= \omega_p - \omega_T \end{aligned} \quad (8)$$

Because humans are not robust and simple, the system describes the rotation of a pitcher's kinematics with the assumption that the angular acceleration is constant. Immediately prior to foot contact, the pelvis will accelerate and rotate at a peak angular velocity at FFC. This action is the primer for separation which is defined by the angle of the pelvis minus the angle of the thorax. This also means that when our pelvis and thorax are lined up with each other, the angle of separation is 0° , and our spring is at equilibrium. There are 2 approaches to



FIG. 2: Rōki Sasaki: An elite 21 yr. old Pitcher from Team Japan. At $t = FCC$, the separation angle is open and $\omega_{sep,FCC} = \omega_p$. at $t = MER$, the separation angle is closed thus approaching the boundary condition of $\omega_{sep,MER} = \omega_T$ and $\theta_{sep,MER} = 0^\circ$.

the torsional spring model from FFC to MER. This assumes that $\theta_{sep,MER} = 0^\circ$ rather than the torso rotating past the pelvis. When looking at the Energy approach the damping effect is built into the ratio of $\frac{K_T}{I}$. As the pitcher continues to throw, the athlete will not close separation efficiently, therefore having a smaller ratio due to muscular fatigue; therefore, the assumption is that energy from FCC to MER is conserved.

$$E_{FCC} = E_{MER} \quad (9)$$

When looking at the energy between foot contact and external rotation, the potential and kinetic energy both use the separation angle and separation angular velocity defined previously in Equation ??.

$$\frac{1}{2} K_T \theta_{sep,FFC}^2 + \frac{1}{2} I \omega_{sep,FFC}^2 = \frac{1}{2} K_T \theta_{sep,FFC}^2 + \frac{1}{2} I \omega_{sep,MER}^2 \quad (10)$$

After rearranging like terms, the ratio of the torsion constant and the moment of inertia can be constructed.

$$\frac{K_T}{I} = \frac{\omega_{sep,FCC}^2 - \omega_{sep,MER}^2}{\theta_{sep,MER}^2 - \theta_{sep,FFC}^2} \quad (11)$$

This energy approach is still incomplete. the energy within a pitcher is not conserved and thus needs to be re-modeled with this approach as the basis for an improved model. For this study, a Kinematic approach will be used to describe the motion of the torsion spring. First the angular acceleration is defined using the governing kinematic equation.

$$\begin{aligned} \omega_{sep,MER}^2 - \omega_{sep,FFC}^2 &= 2\alpha(\theta_{sep,MER} - \theta_{sep,FFC}) \\ \omega_{sep,MER}^2 - \omega_{sep,FFC}^2 &= 2\alpha\Delta\theta_{sep,FFC} \end{aligned} \quad (12)$$

The boundary conditions of our spring are defined where $\omega_{sep} = \omega_p$ at $t = FCC$, and during $t = MER$, $\omega_{sep} = \omega_T$. Using these boundary condition, Equation 12 can be rewritten as

$$2\alpha = \frac{\omega_{sep,MER}^2 - \omega_{sep,FFC}^2}{\Delta\theta_{sep,FFC}} \quad (13)$$

After finding angular acceleration, an equation for the torque due to torsion is derived

$$\sum \tau = RK_T \Delta\theta_{sep} \quad (14)$$

where K_T is the torsion constant, $\Delta\theta_{sep}$ is the separation angle defined by in Equation 8, and R is the distance from our axis of rotation or the radius of the spring (Note: K_T has an . Because pitchers rotate through the center of their body, R is the radius of their pelvis.

By solving for torque, the 2α found earlier can be substituted to derive the system

$$\begin{aligned} 2RK_T \Delta\theta_{sep} &= 2I\alpha \\ 2RK_T \Delta\theta_{sep,FFC} &= I \frac{\omega_{sep,MER}^2 - \omega_{sep,FFC}^2}{\Delta\theta_{sep,FFC}} \end{aligned} \quad (15)$$

After rearranging some terms, a value for $\frac{K_T}{I}$ is derived with the assumption that α is constant throughout our system.

$$\frac{K_T}{I} = \frac{1}{2R} \frac{\omega_{sep,MER}^2 - \omega_{sep,FFC}^2}{\Delta\theta_{sep,FFC}^2} \quad (16)$$

Finally after defining a damping constant for the critically damped case, the equation for the critically damped oscillator is constructed using the 2 angular amplitudes of separation, the damping constant, and a time series to model the angular position of the torsion spring.

$$\theta_{sep}(t) = (A - Bt)e^{-\alpha t} \quad (17)$$

Experimental Details

This study is a prospective cohort approved by the university institutional review board to describe a model for energy flow of the torso in a collegiate pitcher. All participants had access to experimental procedures and signed informed consent and gave verbal assent. All participants were selected under the following inclusion criteria: Enrolled in RIT and apart of the university baseball team in the fall 2022, Familiar with pitching mechanics, pain free, Participating in all games and practices, cleared by an athletic trainer or medical physician through a physical. Athletes were excluded under the following criteria: Fails to participate in all games or practices, Current pain with throwing, Fails to pass a physical. A total of 12 participants were selected from the RIT pitching staff from the fall of 2022.

After participant self selected warm up during practice, participants will throw a bullpen as instructed by the RIT pitching coach. 3D motion capture data were collected using ProplayAi, an iOS application utilizing the iPhone camera application slow motion feature. 12 AI markers are placed on the joint segments required for joint kinematic calculations. Motion capture data were



FIG. 3: The ProplayAi interface tracking body kinematics along with key velocity contributors on the side.

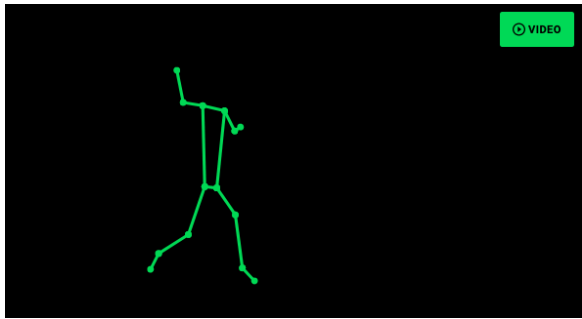


FIG. 4: The ProplayAi interface tracking body kinematics along with key velocity contributors on the side.

collected at 200 Hz. Individualised ball kinematics were collected using a Rapsodo recording at 300Hz. Each participant had 2-5 trials recorded for each pitch that were then averaged into one pitch report. Rotational kinematics and KPI's were recorded from averaged reports. Pitch Types used in this study are listed as followed: Fastball (FS), 2-Seam Fastball (2S), Cutter (CU), Curveball (CB), Change-Up (CH), Slider (SL), Split-Finger (SP), and Knuckle-ball (KN). All data were collected during the months of October and November of 2022.

Phase Portraits were made for each participant using the decoupled system demonstrated in Equations 7. A trajectory for each pitch type is modeled from the dot representing FFC, to the fixed point defined by the nulcline intersection at (0,0) at MER. Time is moving right to left. Each initial dot is in the form of $(\theta, \dot{\theta})$. To match the dimensionless form of the equation, all angular velocities were recalculated by dividing $\theta_{sep,i}$ by the constructed dimensionless time in Equation 5 where $\tilde{t} = \sqrt{\frac{K_T}{T}}$ and is calculated using Equation 4

Exponential decay time series of Equation 17 are plotted for each participant. The value for α is calculated using Equation 4 and values for A and B in Equation 17 are evaluated using the boundary conditions at θ and $\dot{\theta}$ at $t = FFC$ and $t = MER$.

A statistical analysis will compare α to KPI values using a linear regression model, along with a residuals

to describe the accuracy of the linear model. R^2 values along with regression lines will be reported.

Analysis

When looking at the rotation of the each participant, the angular frequency α is dependent on both $\theta_{sep,i}$ and $\omega_{sep,i}$. A phase portrait of the ω_{sep} vs θ_{sep} can be constructed for each participant using the decoupled Equations 7. The trajectory of the phase portrait maps from the dot representing the $\dot{\theta}$ and θ at FFC, to the fixed point defined by the nulcline intersection at (0,0) at MER.

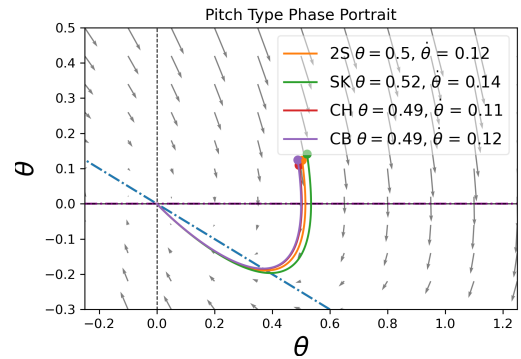


FIG. 5: An elite pitcher phase portrait with trajectories for each pitch type. As $\dot{\theta}$ is positive and farther from the nulcline, the athlete at FFC is moving faster causing a more efficient rotational trajectory.

Time moves right to left as the dot represent $t = FCC$ and the fixed point (0,0) represents $t = MER$. When the initial values at FFC start farther away from the nulcline, $\dot{\mu} = 0$, $\dot{\theta}$ becomes a larger positive value. The corresponding value on the vector field shows that athletes that start farther from the nulcline have a velocity with a higher magnitude. Therefore, when athlete begins their rotation farther from the nulcline in the positive direction, the magnitude of the velocity arrow describes a faster moving athletes, which corresponds with higher ball velocities. At FFC, a positive value for $\dot{\theta}$ describes an athlete that rotates with their pelvis first.

When the value is negative the athlete rotates with their thorax faster than their pelvis. The torso cannot properly separate when the thorax moves faster at $t = FCC$, which causes the torso to move with a slower velocity. Therefore, when the pelvis does not rotates faster than the thorax at FFC, the athlete cannot utilize the elastic properties of the torso to accelerate their arm into ball release. Thus the farther the point is from the nulcline, the faster the athlete is rotating at the initial condition. For an athlete to create efficient rotation, both $\dot{\theta}$ and θ must increase in the positive direction.

A plot of the time series for an elite participant using Equation 17. As outlier faster moving athletes dis-

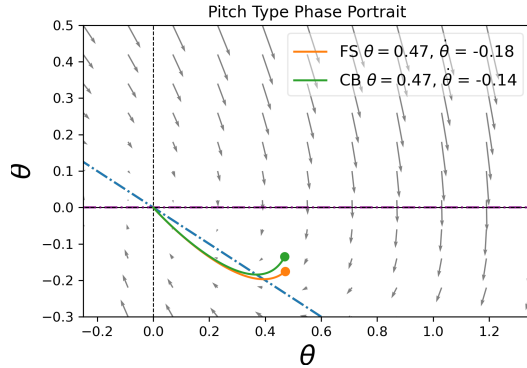


FIG. 6: An non-elite pitcher phase portrait with trajectories for each pitch type. As $\dot{\theta}$ is negative and closer to the nulcline, the athlete at FFC is moving slower causing a non-efficient rotational trajectory.

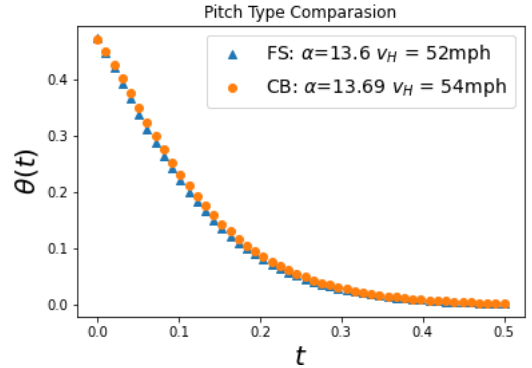


FIG. 8: A time series for the critically damped oscillator using Equation 17. A small α corresponds to a slower rate of rotation. Participant has the following pitch arsenal: Fastball (FS) and Curveball (CB).

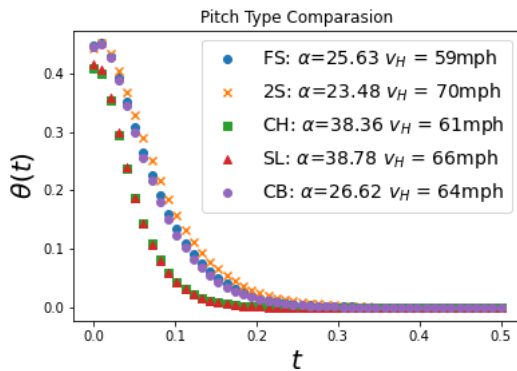


FIG. 7: A time series for the critically damped oscillator using Equation 17. A larger α corresponds to a faster rate of rotation. Participant has the following pitch arsenal: Fastball (FS), 2-Seam Fastball (2S), Change-Up (CH), Slider (SL), and Curveball (CB).

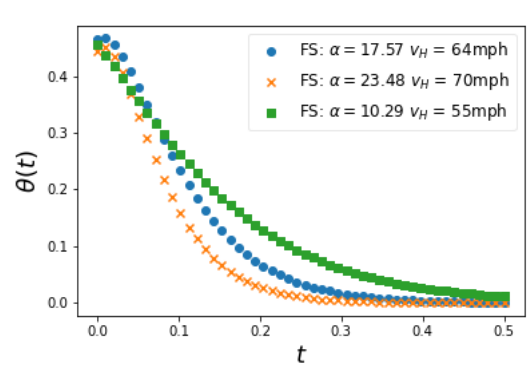


FIG. 9: A time series for the critically damped oscillator using Equation 17 for 3 different athletes. As the value for α increase, the quicker we approach 0° and the faster the athlete rotates into MER. Faster rotation leads to a faster arm acceleration into BR.

play a larger damping constant, the separation angle approaches 0° fairly quickly. A larger damping constant corresponds to a faster hand velocity as the torso accelerates the arm faster through the throwing plane.

A plot of the time series for an non-elite participant using Equation 17. As slower moving outlier athletes display a smaller damping constant, the separation angle takes more time to approaches 0° agree when compared to an elite athletes rotation. A smaller damping constant demonstrates a slower hand velocity as the torso accelerates the arm faster through the throwing plane. A time series for 3 different participants is plotted using Equation 17 for different values of α . Each values for α showcase 3 different rotational trajectories for each athlete types. As the value for α increases, $\theta(t)$ approaches 0° much faster. A further discussion for $\alpha = 17.59$ and $\alpha = 25.48$ will be further explored.

A statistical model for α vs v_{hand} was analyzed using a linear regression model. The blue line represents

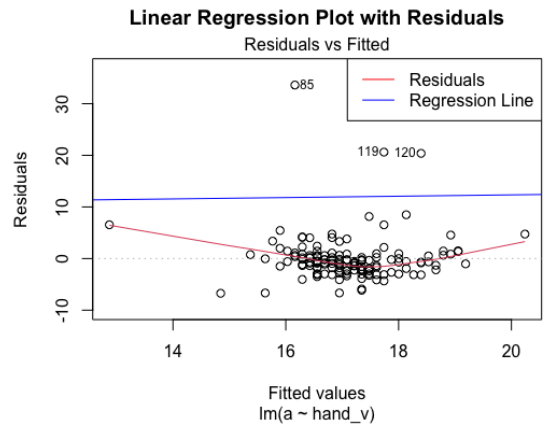


FIG. 10: The linear regression model of αv_{hand} demonstrated an Adjusted R^2 value of 0.03258 and a linear fit of $a = 9.71 + 0.13V_H$

the linear regression line. The red line is a residuals displayed using the linear fit as the predicted model. The R^2 demonstrates no correlation between the damping constant α and v_{hand} .

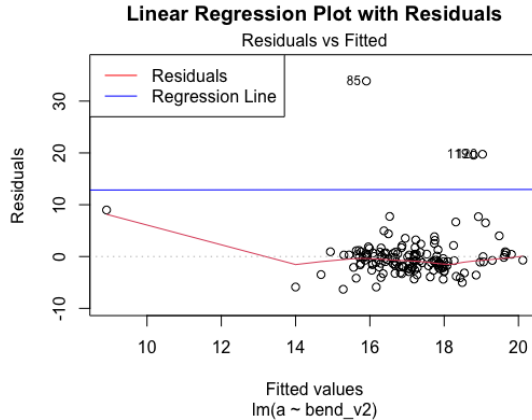


FIG. 11: The linear regression model of α vs v_{bend} demonstrated an Adjusted R^2 value of 0.07515 and a linear fit of $a = 12.76 + 0.54V_{bend}$

A statistical model for α vs v_{bend} (torso flexion velocity) was analyzed using a linear regression model. The blue line represents the linear regression line. The red line is a residuals displayed using the linear fit as the predicted model. The R^2 demonstrates no correlation between the damping constant α and v_{bend} .

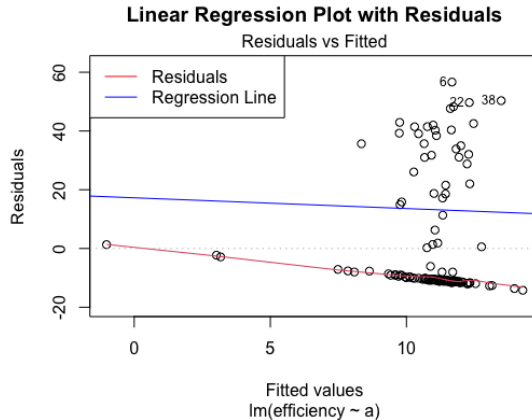


FIG. 12: The linear regression model of Efficiency vs α demonstrated an Adjusted R^2 value of 0.000825 and a linear equation of $a = 17.26 - 0.37 * EFF$. Efficiency is defined by arm speed divided by torque as a percentile of the ProplayAi database. $\frac{v_{arm}}{\tau_{elbow}}$

A statistical model for α vs Efficiency was analyzed using a linear regression model. The blue line represents the linear regression line. The red line is a residuals displayed using the linear fit as the predicted model. The R^2 demonstrates no correlation between the damping constant α and Efficiency.

stant α and v_{bend} . A statistical model for α vs Stride



FIG. 13: The linear regression model of α vs Stride Length demonstrated an Adjusted R^2 value of -0.005718 and a linear equation of $a = 12.76 + 0.54(stride)$. Stride Length is defined by the distance of back foot to front foot as a percentage of body height.

Length was analyzed using a linear regression model. The blue line represents the linear regression line. The red line is a residuals displayed using the linear fit as the predicted model. The R^2 demonstrates no correlation between the damping constant α and Stride Length.

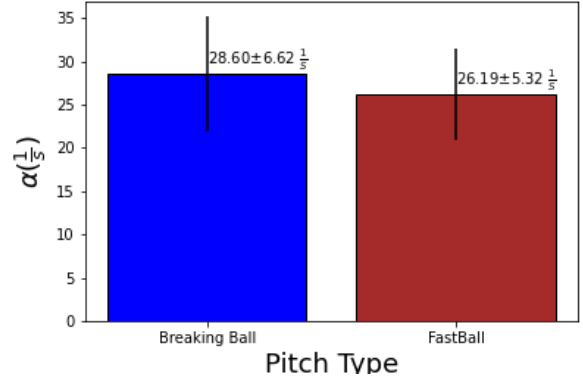


FIG. 14: When graphing the α means from the ANOVA test, the observed values for the mean are shown for Fastballs and Breaking Balls. Mean Values: $FS = 296.30 \pm 78.93$, $BB = 233.08 \pm 51.31$. The p-value of the ANOVA: $p=0.02$

An ANOVA of the entire data set from Fall 2022 demonstrated no statistical significance amongst α and pitch type category. The fastball category were comprised of all 4-Seam and 2-Seam Fastballs. The Breaking Ball category were all other pitches that were not included for the Fastball category. Each player has more breaking pitches than fastballs in their pitching arsenal. A p-value of 0.02 demonstrates a statistical significance between α and pitch type.

Discussion

When comparing Figures 6-7 to Figures 8-9, an observational analysis can be made between the damping constant and the trajectories of the phase space. The phase portrait models torso rotation by having the larger $\theta_{sep,i}$ with a corresponding larger $\omega_{sep,i}$. If all of these conditions are not met, then the trajectory can be identified as non efficient. This is represented by the magnitude of the vector field at the instantaneous point of front foot contact (FFC). The farther out the point is the faster the elastic properties accelerate the torso into equilibrium. The exponential decay plots describe the rotation based on the α value. When α is large, the torso will approach 0° fairly quickly compared to smaller counterparts. It is safe to observe that a group of elite throwers that have a large positive $\theta_{sep,i}$ and $\omega_{sep,i}$, will also have a large corresponding α value.

When comparing the plots in Figure 10, The two alpha values read $\alpha = 17.59$ and $\alpha = 25.48$. Although the values for alpha are different, the hand velocities are very similar. This is a phenomenon known as effortless velocity. When an athlete throws with their body using the elastic properties of their core, they take more of the load off their arm, and throwing the ball becomes "effortless". When an athlete throws using their arm and not their body, they will add more elbow varus torque on their throwing arm which causes the UCL to tear. Thus the larger the damping constant, the more the athlete is using their body and the small the kinetics are on the throwing arm.

The statistical analysis in the previous section determined that there was a statistical significance amongst α to pitch type. With the mean values being larger for the breaking balls, there are two options. Either the athletes are utilizing more of their elasticity when throwing a breaking ball, or the MOI is smaller by the mass of the torso is more displaced closer to the axis when compared to the fastball.

None of the KPI values had a linear correlation to the damping constant α . This could be interpreted a couple different ways. 1. No KPI values have any correlation to α . If nothing were correlated at all, this would mean one of two outcomes. Either the model for finding the Damping Constant is missing a very vital key component, or rotation does not matter when it comes to throwing. A study done by Cohen, et al² demonstrated that an increase in torso maximum rotational velocity was significantly associated with increasing the ball velocity. This validates that rotation is heavily crucial when it comes to ball velocity predictors. Also because both pelvis and thorax are a part of the kinetic chain of the pitching delivery, it is safe to assume that torso rotation matters a great deal. The model used to find the damping constant could be improved from a 1 degree of freedom model to a 3 degrees of freedom model. The damping constant is derived from motion only happening in the transverse plane. The pitching delivery is a multi-planar movement where there

is rotation happening in all 3 planes of motion (sagittal, frontal, and transverse). Another study published by Crotin, et al³ demonstrated a smaller lateral trunk (torso) tilt corresponded to a higher ball velocity and biomechanical efficiency. At the division 3 level, athletes do not have the proper mechanical background or coaching needed to play at the Division 1 level, therefore, our data-set could be missing this component of motion when describing how the torso could be damped as it relates to a trunk lateral and forward tilt angles and velocities to better map how the energy is dispersed throughout the entire mass distribution of the torso (trunk). While model improvements are needed to further this research, a 1D base model should still have some significance if the study by Cohen et.al² showed a statistical correlation with our 1D variables used to calculate α .

2. The data collected is insufficient in making any concrete conclusions. There is a lot to unpack here. ProplayAi is a 2D model that tracks the joint kinematics based on AI generated joint segments. While some metrics such as stride length can have some validity because of its 1D nature, any type of rotation from the transverse plane is very difficult for ProplayAi to track with validity. A laboratory setting will have a 41 retro-reflective marker set with 12 cameras above the athlete. This allows the technology to track the skeleton in all movement planes in a 3D space.



FIG. 15: An RIT athlete kinematic sequence data taken using 4D motion sensor technology

A sensor setting also tracks the 3D motion by being visibly on the body similarly to a marker set, but with a built in gyroscope and accelerometer in X, Y, and Z. ProplayAi attempts to track the missing Z-direction, without any assistance from any other angle or perspective, thus not being able to identify rotation as accurately as the other technologies out there.

To add onto the technological challenges, the RIT coaching staff presented external push back that caused limitations. These limitations include consistent access to participants involvement in data collection. This involves each data collection sessions having an inconsistent number of participants to participate in data collection. The RIT coaching staff also had control over participants involvement in data collection, thus each participants have an inconsistent pitch reports per week. This

is because the IRB was designed to be a non-intervention study. Future studies should involve pitch type interventions in order to keep participant data more consistent.

Conclusion

In conclusion, No KPI's showed any statistical significance when compared to the damping constant α . Although the Critically damped models using Equations 17 demonstrated correlation in outlier cases, Values for α need to be reexamined using 3D motion capture data in order model the rotation with more precision. Phase portraits demonstrated the rotation between FFC and MER. Curvature of trajectory for each pitch type may quantify a direct correlation with the calculated α quantified Equation 4.

When reexamining the model, all degrees of freedom must be accounted for before constructing the torsion oscillator. A change in technology must also be accounted for when reexamining the study in a laboratory setting, or a competitive setting using wearable sensors. Before changing a statistical model, reevaluated data should be run through the same statistical analysis to examine linear dependence.

This study will be continued at Louisiana Technol-

ogy under the Human Movement Laboratory. It will be part of a Masters thesis consisting of individualized torso mass distributions using a DEXA-scan for each participant, along with more precise modeling to calculate α with multiple degrees of freedom. A laboratory and competitive setting will be conducted to measure fatigue and adrenaline effects of the rotational kinematics of the torso between the two environments. Also, a biomechanical efficiency analysis will be conducted to analyze performance with torso kinematics.

Acknowledgments

Thank you to my Faculty Advisors, Dr. Dawn Hollenbeck and Professor William Brewer, for supporting the project and guidance to jump-start something new at RIT. I couldn't have asked for better capstone advisors who have fought tooth and nail along side me this last year. Also a special thanks to Dr. Michael Pierce and the capstone committee for allowing me the opportunity of exploring biomechanics, it was the ripple effect that shaped my RIT experience and who I am today. Thank you to all of the RIT pitcher participants who took part in this study.

- * Rochester Institute of Technology, School of Physics and Astronomy, Faculty Advisor: Dawn Hollenbeck, Bill Brewer
- ¹ Aguinaldo, Arnel and Nicholson, Kristen (2021) "LOWER BODY CONTRIBUTIONS TO PELVIS ENERGY FLOW AND PITCH VELOCITY IN COLLEGIATE BASEBALL PLAYERS," ISBS Proceedings Archive: Vol. 39: Iss. 1, Article 36. Available at: <https://commons.nmu.edu/isbs/vol39/iss1/36>
- ² Cohen AD, Garibay EJ, Solomito MJ. The Association Among Trunk Rotation, Ball Velocity, and the Elbow Varus Moment in Collegiate-Level Baseball Pitchers. *Am J Sports Med.* 2019 Oct;47(12):2816-2820. doi: 10.1177/0363546519867934. Epub 2019 Aug 19. PMID: 31424975.
- ³ Crotin RL, Slowik JS, Brewer G, Cain EL, Fleisig GS. Determinants of Biomechanical Efficiency in Collegiate and Professional Baseball Pitchers. *The American Journal of Sports Medicine.* 2022;50(12):3374-3380. doi:10.1177/03635465221119194.
- ⁴ Fleisig GS, Diffendaffer AZ, Ivey B, Oi T. Do Mound Height and Pitching Distance Affect Youth Baseball Pitching Biomechanics? *The American Journal of Sports Medicine.* 2018;46(12):2996-3001. doi:10.1177/0363546518795890
- ⁵ Fortenbaugh D, Fleisig GS, Andrews JR. Baseball pitching biomechanics in relation to injury risk and performance. *Sports Health.* 2009 Jul;1(4):314-20. doi: 10.1177/1941738109338546. PMID: 23015888; PMCID: PMC3445126.
- ⁶ Hulbert T, Catalano T, Nicholson KF. Comparison of OnBaseU Tests with Biomechanical Motion Analysis in Youth Baseball Pitchers. *Int J Sports Phys Ther.* 2021 Dec 1;16(6):1513-1522. doi: 10.26603/001c.29519. PMID: 34909256; PMCID: PMC8637262.
- ⁷ Michael E. O'Connell, Kyle E. Lindley, John O. Scheffey, Alex Caravan, Joseph A. Marsh, Anthony C. Brady. (2022) Weighted Baseball Training Affects Arm Speed Without Increasing Elbow and Shoulder Joint Kinetics. *Journal of Applied Biomechanics* 38:5, 281-285. Online publication date: 1-Oct-2022.
- ⁸ Seroyer, Shane & Nho, Shane & Bach, Bernard & Bush-Joseph, Charles & Nicholson, Gregory & Romeo, Anthony. (2010). The Kinetic Chain in Overhand Pitching: Its Potential Role for Performance Enhancement and Injury Prevention. *Sports health.* 2. 135-46. 10.1177/1941738110362656. View [30 April 2022].

Appendix A

Name:	Age:	Date:	
Hits RT LT	Throws RT LT	Weight:	Height:
Pelvic Tilt	Toe Tap Test	Side Step Walkout Test	Half-Kneeling Narrow Base
Athletic Posture (Subjective)	L One Foot Length Apart	R	Shoulder 90/90
Neutral Tilt	Touches	Part Ball	Standing Tall
S-Posture	Short	Equal to Ball	Greater than Spine Angle
C-Posture	L Holding Pelvis	R Less than Ball	Unstable
Amount of Motion	Improves	Push-Off Test	Equal to Spine Angle
Normal Motion	No Change	Lunge w/ Extension Test	Less than Spine Angle
Hard Time Arching Back	Hip 45 Test	> 6 Foot Length	Windshield Wiper Test
Hard Time Flattening Back	L 45 Degree Angle	R 5-6 Foot Lengths	In Front
Both Limited	Greater than 45 degrees	< 5 Foot Lengths	Can Get into Starting Position
Quality of Movement	Equal to 45 Degrees	Part I - Normal Throw	= or > 90°
Smooth Movement	Less than 45 Degrees	> 1 Foot Length Increase	Can't Get into Starting Position
Shake and Balance Movement	Seated Trunk Rotation	5-1 Foot Length Increase	= or > 90°
Did Not Test	L Bent Behind Neck	R < 3 Foot Length Increase	Shoulders Don't Clear Hip Thigh
Pelvic Rotation	Greater than 45 degrees	Heel Lift Test	Least Shoulder Flexion
L Without Holding Shoulders	R Equal to 45 degrees	L Height of Lift	Forearm 80/80 Test
Good	Less than 45 degrees	R Good L/R	Wide Squat Test
Limited	R Turning Head	L Limited Lift	L Palm Towards (Curve)
L Holding Shoulders	R Good - Over Glide	R Quality of L/R	R Palm Away (Change Up)
Improves	L Limited - Short of Circles	L Unstable	80 degrees or More
Doesn't Improve		R Unstable	Less than 80 Degrees
L Coordination	R		All Side
Good Rotary Movement			Windshield Wiper Test
More Lateral Movement			Shoulder 90/90
Core Control Gang			Half-Kneeling Narrow Base
Rotation Gang			Lunge with Extension
Stride Gang			Wide Squat
Upright Posture Gang			Windshield Wiper Test
Arm Gang			Forearm 80/80
Normal			ONBASE UNIVERSITY

FIG. 16: OnbaseU Test Sheet

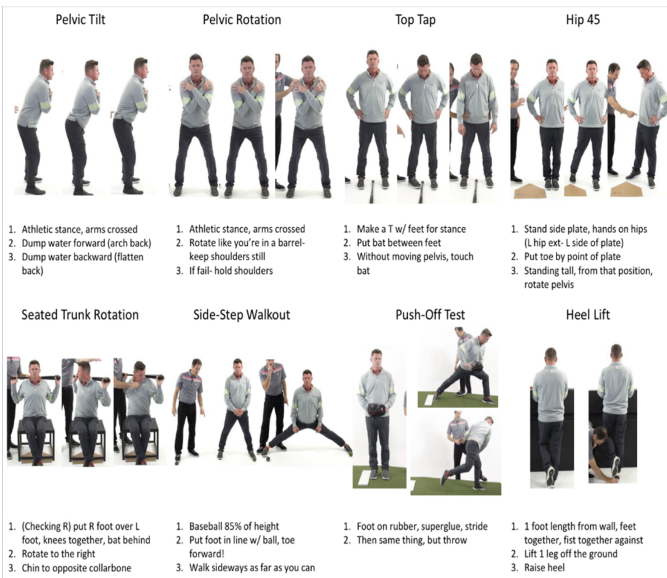


FIG. 17: OnbaseU Protocol 1

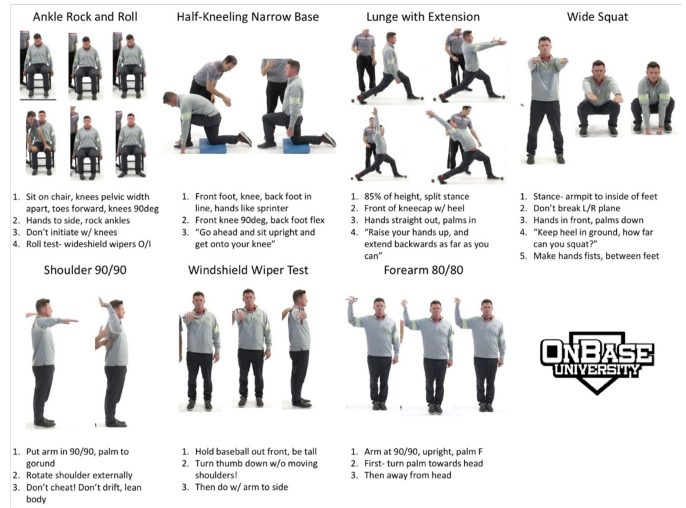


FIG. 18: OnbaseU Protocol 2



FIG. 19: Oats specialist club



FIG. 20: Driveline Plyoball comparison to baseball with weights. A Baseball is 5oz with a 9 inch circumference

Unwinds are a drill used to help an athlete understand the feeling of separation. Separation is obtained by separating the pelvis from the trunk in order to create an elastic stretch throughout the trunk. The purpose of the unwind is to take the lower body mechanics out of the throwing motion. This helps to cue athletes on how to create powerful rotational energy and transfer it efficiently in the direction of your throwing target. To complete the drill, players first must get in a athletic front stance with their trail leg in front and their led leg in the back (on the balls of the foot). Throwing arm will be positioned in the upright position with the arm bent less than 90° to establish scapular engagement and good arm mechanics. After proper positioning, the player will begin to counter rotate their torso while keeping their pelvis forward.



FIG. 21: First stage of unwinds is to coil and stack the trunk into counter rotation Athlete must put pressure on front foot to maximize energy transfer.

This is done by putting pressure on the leg that is in front which produces a ground reaction force into the ground. This counter movement initiate the separation between pelvis and torso which allows the athlete to understand how to utilize the elasticity within their body. As the athlete winds up the separation, they will reach a peak separation due to flexibility range of motion.



FIG. 22: Second Stage of unwinds is to unwind the trunk by letting the tension throughout your body accelerate the system to conserve energy throughout the body.

When peak separation is achieved, the athlete will release the tension throughout the body by letting the body naturally unwind the tension built up. An example of this is when you release a rubber band. Rubber bands are not flung by pushing the rubber band to make it go faster, the band is instead let it go and the tension of the rubber band accelerates the band. Players will do a

progression set of unwinds using an Oats specialist club, Blue Driveline Plyoball, and Red Driveline Plyoball all 8x each. This progression set will give the athletes instant feedback with correctives after each throw.

Appendix B: Phase Portraits and Critically Damp Decay Models

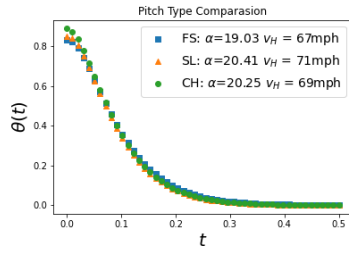


FIG. 23: damp

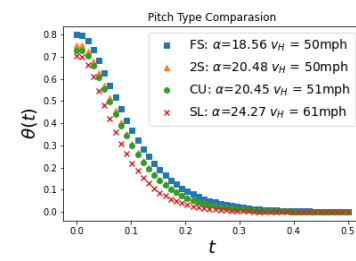


FIG. 27: DAMP

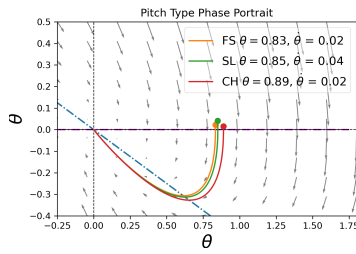


FIG. 24: phase

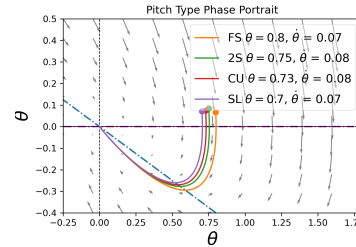


FIG. 28: PHASE

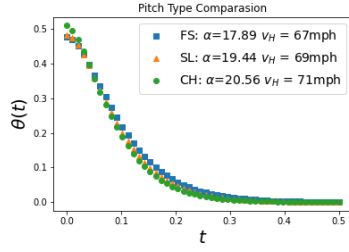


FIG. 25: damp

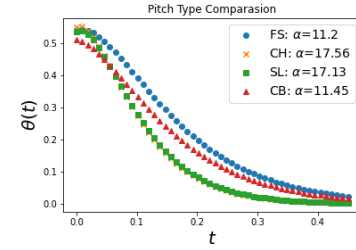


FIG. 29: DAMP

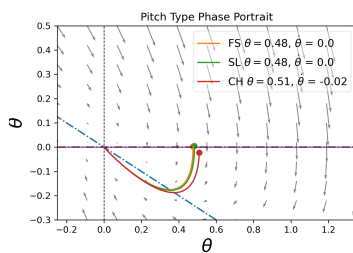


FIG. 26: PHASE

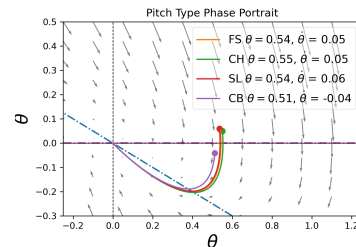


FIG. 30: PHASE

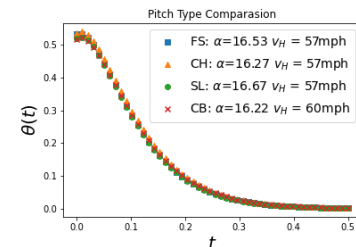


FIG. 31: DAMP

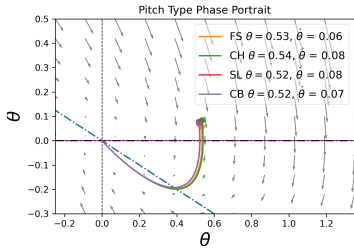


FIG. 32: PHASE

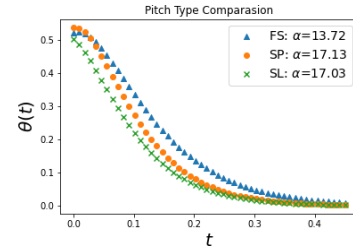


FIG. 37: DAMP

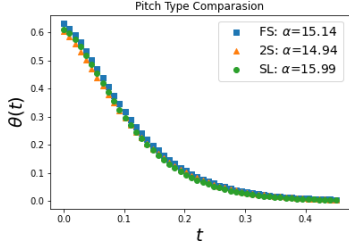


FIG. 33: DAMP

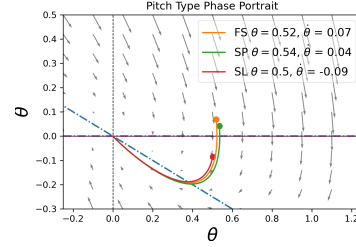


FIG. 38: DAMP

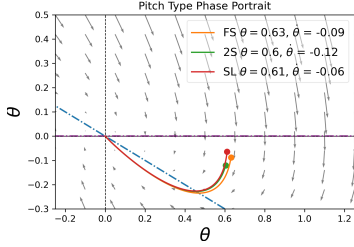


FIG. 34: PHASE

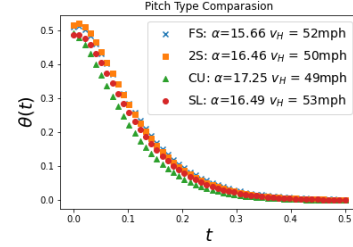


FIG. 39: DAMP

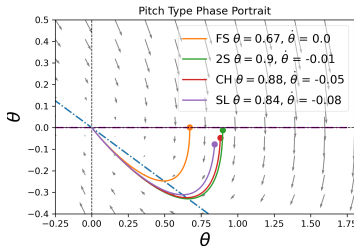


FIG. 35: PHASE

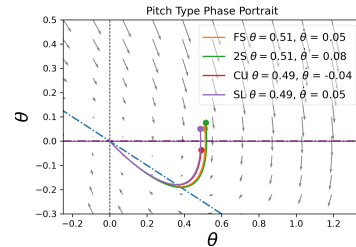


FIG. 40: DAMP

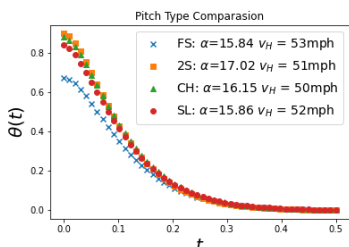


FIG. 36: DAMP

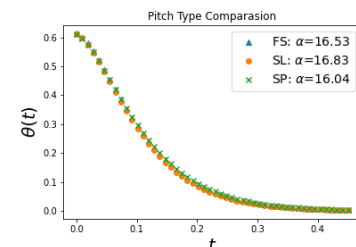


FIG. 41: DAMP

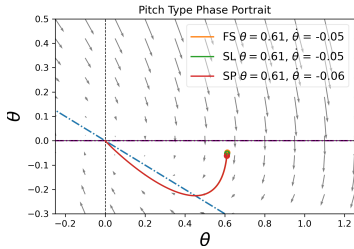


FIG. 42: PHASE

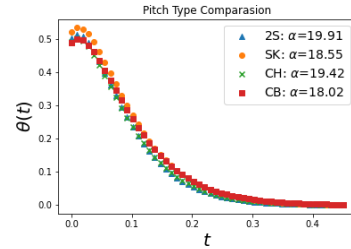


FIG. 47: DAMP

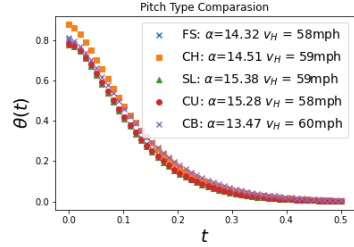


FIG. 43: DAMP

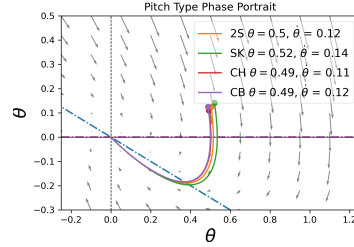


FIG. 48: phase

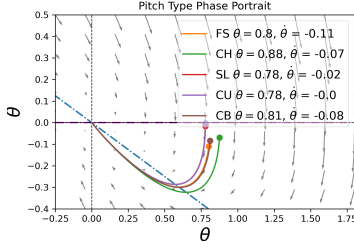


FIG. 44: phase

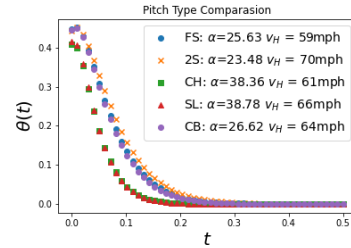


FIG. 49: DAMP

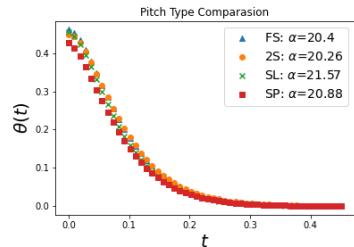


FIG. 45: DAMP

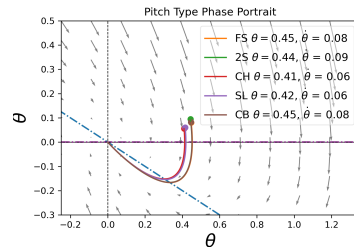


FIG. 50: phase

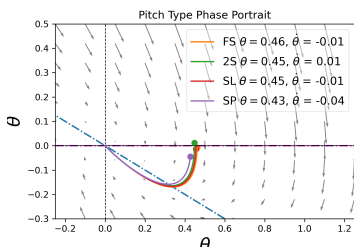


FIG. 46: phase

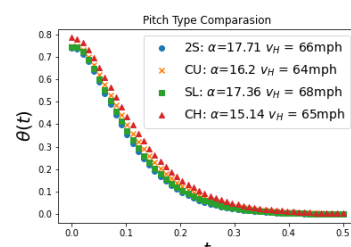


FIG. 51: DAMP

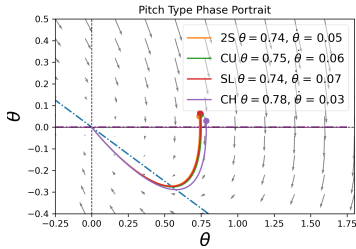


FIG. 52: phase

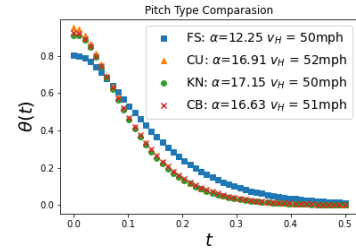


FIG. 57: damp

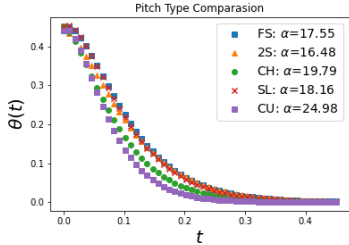


FIG. 53: damp

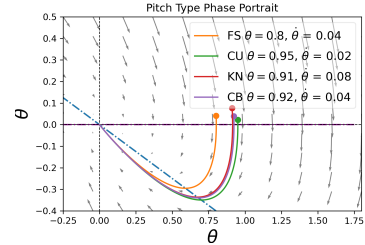


FIG. 58: phase

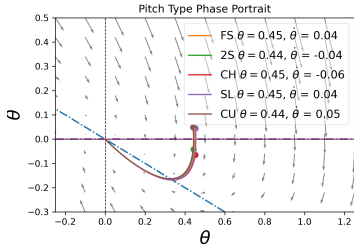


FIG. 54: phase

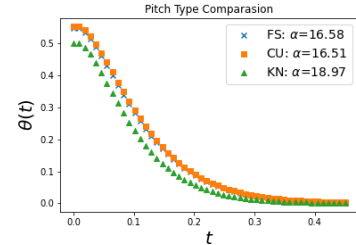


FIG. 59: damp

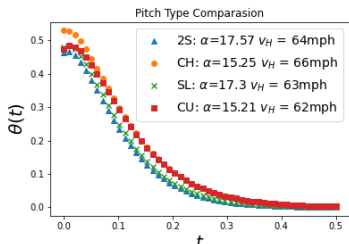


FIG. 55: damp

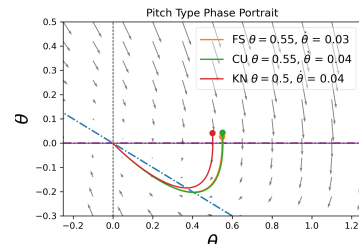


FIG. 60: phase

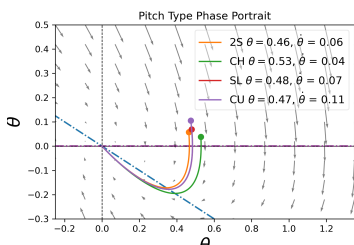


FIG. 56: phase

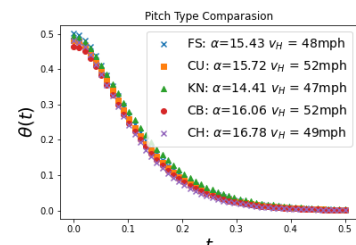


FIG. 61: damp

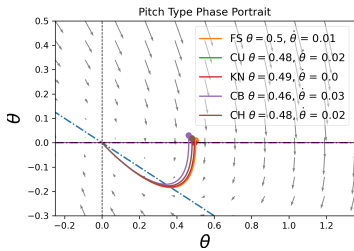


FIG. 62: phase

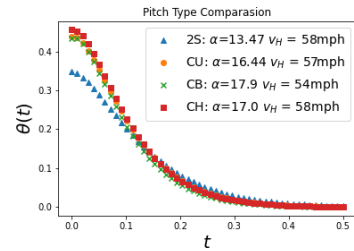


FIG. 67: damp

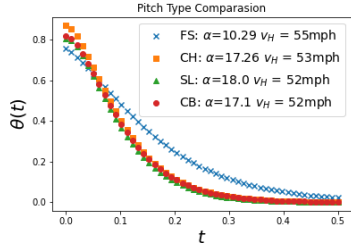


FIG. 63: damp

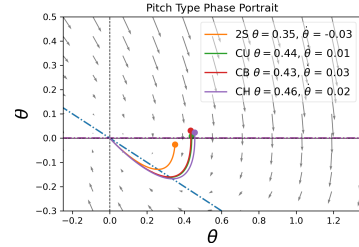


FIG. 68: phase

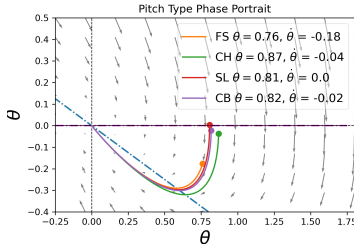


FIG. 64: phase

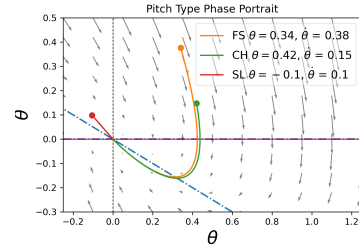


FIG. 69: phase

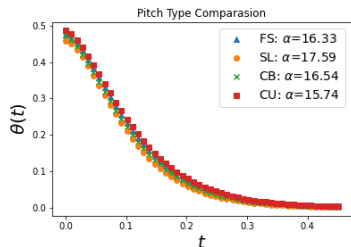


FIG. 65: damp

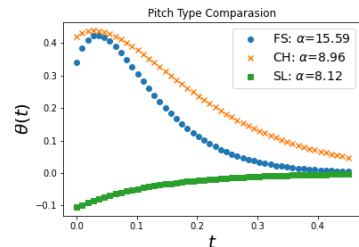


FIG. 70: phase

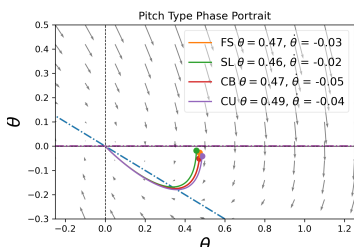


FIG. 66: phase

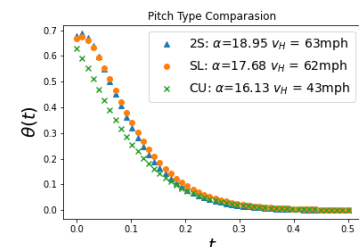


FIG. 71: damp

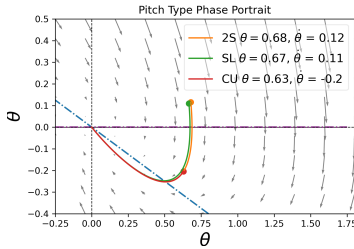


FIG. 72: phase

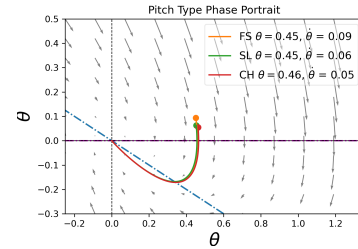


FIG. 76: phase

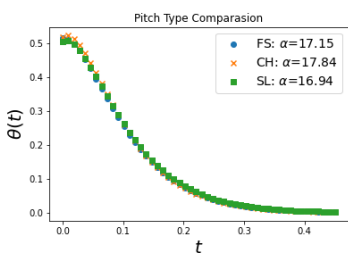


FIG. 73: damp

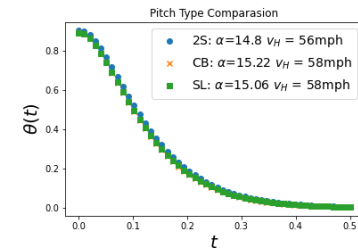


FIG. 77: damp

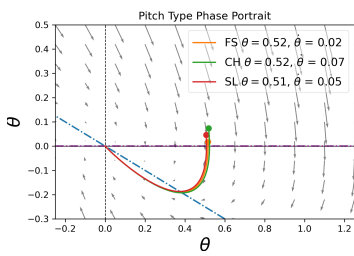


FIG. 74: phase

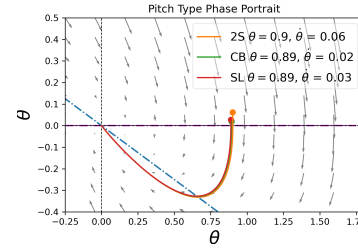


FIG. 78: phase

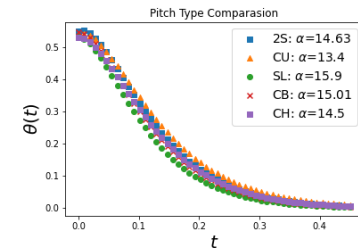


FIG. 79: damp

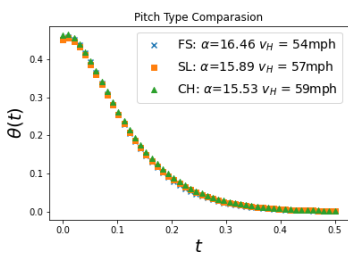


FIG. 75: damp

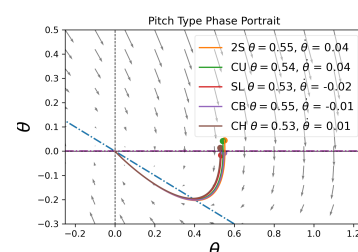


FIG. 80: phase

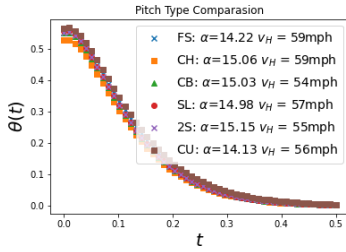


FIG. 81: damp

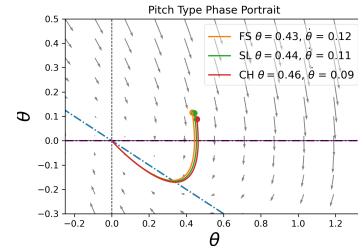


FIG. 86: phase

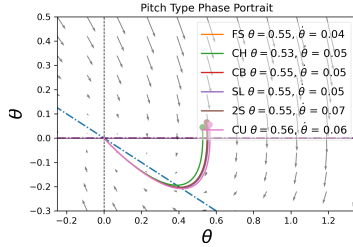


FIG. 82: phase

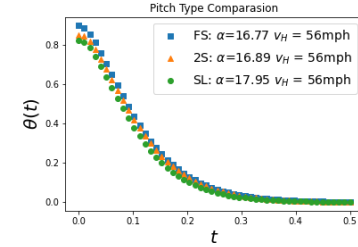


FIG. 87: damp

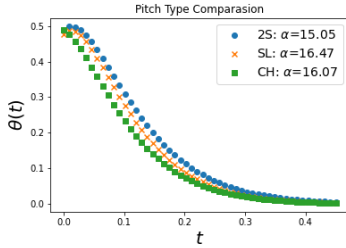


FIG. 83: damp

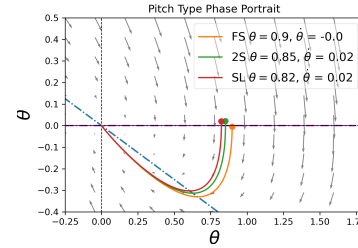


FIG. 88: phase

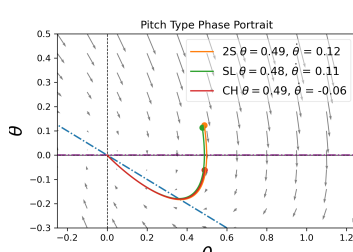


FIG. 84: phase

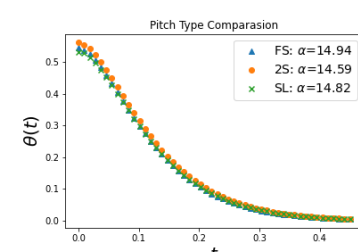


FIG. 89: damp

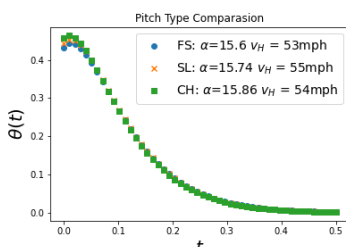


FIG. 85: damp

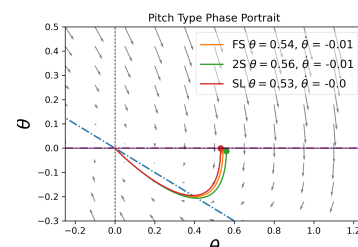


FIG. 90: phase

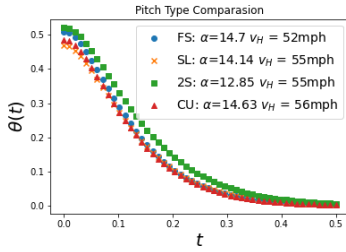


FIG. 91: damp

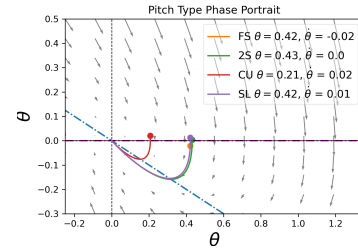


FIG. 96: phase

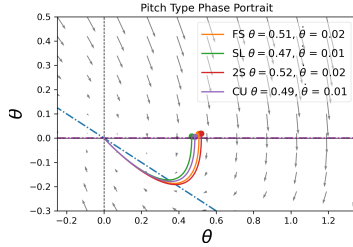


FIG. 92: phase

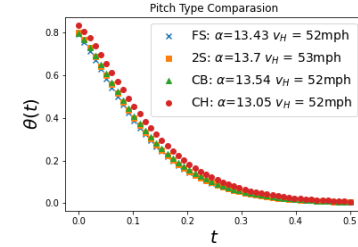


FIG. 97: damp

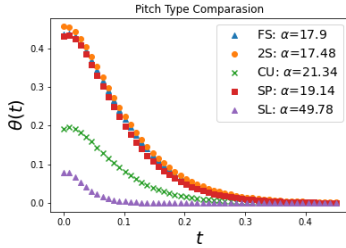


FIG. 93: damp

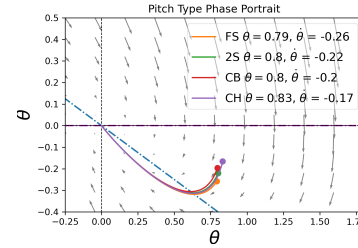


FIG. 98: phase

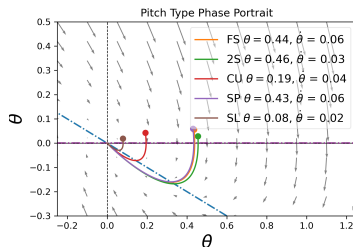


FIG. 94: phase

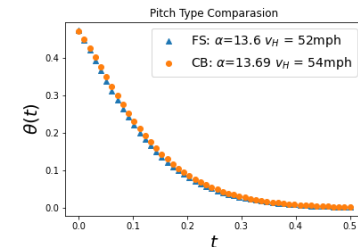


FIG. 99: damp

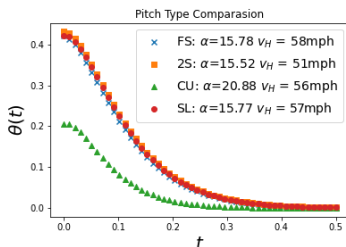


FIG. 95: damp

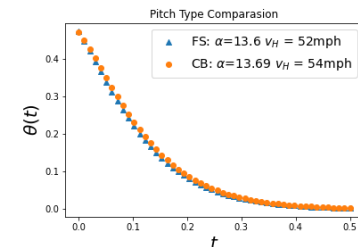


FIG. 100: phase